Observations of spatial flow patterns at the coral colony scale on a shallow reef flat

James L. Hench[1] and Johanna H. Rosman[2]

Received 22 July 2012; revised 31 December 2012; accepted 28 January 2013; published 12 March 2013.

[1] Although small-scale spatial flow variability can affect both larger-scale circulation patterns and biological processes on coral reefs, there are few direct measurements of spatial flow patterns across horizontal scales <100 m. Here flow patterns on a shallow reef flat were measured at scales from a single colony to several adjacent colonies using an array of acoustic Doppler velocimeters on a diver-operated traverse. We observed recirculation zones immediately behind colonies, reduced currents and elevated dissipation rates in turbulent wakes up to 2 colony diameters downstream and enhanced Reynolds stresses in shear layers around wake peripheries. Flow acceleration zones were observed above and between colonies. Coherent flow structures varied with incident flow speeds; recirculation zones were stronger and wakes were more turbulent in faster flows. Low-frequency (<0.03 Hz) flow variations, for which water excursions were large compared with the colony diameters (Keulegan-Carpenter number, $KC > 1$), had similar spatial patterns to wakes, while higher-frequency variations (0.05–0.1 Hz, $KC < 1$) had no observable spatial structure. On the reef flat, both drag and inertial forces exerted by coral colonies could have significant effects on flow, but within different frequency ranges; drag dominates for low-frequency flow variations and inertial forces dominate for higher-frequency variations, including the wave band. Our scaling analyses suggest that spatial flow patterns at colony and patch scales could have important implications for both physical and biological processes at larger reef scales through their effects on forces exerted on the flow, turbulent mixing, and dispersion.

Citation: Hench, J. L., and J. H. Rosman (2013), Observations of spatial flow patterns at the coral colony scale on a shallow reef flat, *J. Geophys. Res. Oceans*, *118*, 1142–1156, doi:10.1002/jgrc.20105.

1. Introduction

[2] It is well recognized that water motion, from colony scale to reef scale, is important for the functioning of coral reefs [*Monismith*, 2007; *Hearn*, 2011]. At the reef scale, flow patterns affect fluxes of nutrients and carbon and hence reef metabolism and calcification rates [*Wyatt et al*., 2010; *Zhang et al*., 2012]. Reef-scale circulation also affects larval retention, export, and connectivity between reefs [*Cowen and Sponaugle*, 2009]. At smaller scales, flow and turbulence adjacent to corals affects nutrient uptake rates [*Thomas and Atkinson*, 1997; *Falter et al*., 2004; *Falter et al*., 2007], gas exchange [*Patterson et al*., 1991; *Sebens et al*., 2003; *Mass et al*., 2010], and the ability of coral polyps and filter feeders to capture particles [*Sebens et al*., 1998]. Turbulent mixing and bed shear stresses also affect the ability of larvae to settle on surfaces [*Reidenbach et al*., 2009]. Moving water also exerts forces on organisms and thus affects the susceptibility to breakage or dislodgement of corals and algae and the energetic cost of occupying a given position on a reef [e.g., *Madin and Connolly*, 2006]. Flow can also mediate rates of coral recovery from corallivory and disturbances [*Lenihan and Edmunds*, 2010]. Because many coral reef organisms are sessile or have a very small range, persistent spatial flow patterns can structure their distributions [*Edmunds et al*., 2010].

[3] While individual organisms are affected by flow conditions at particular positions on coral reefs, most previous field studies of water movement over reefs have focused on regional and lagoon-scale processes [e.g., *Gourlay and Colleter*, 2005; *Hench et al*., 2008; *Lowe et al*., 2009a; *Lowe et al*., 2009b]. The bottom is typically treated like a flat plate with surface roughness, and its effects on flow approximated using roughness length scales [*Reidenbach et al*., 2006; *Hearn*, 2011]. However, the physical structure of a coral reef is complex and reef topography varies continuously across many decades of spatial scales, from centimeters to kilometers [*Zawada et al*., 2010; *Jaramillo and Pawlak*, 2011], and can occupy anywhere from <1% to 100% of the water depth. If most of the flow occurs above the coral canopy layer, then the bottom boundary condition is typically thought of as a shear stress on the overlying flow. In this case, roughness length scales are suitable for

[1]Nicholas School of the Environment, Duke University Marine Laboratory, Beaufort, North Carolina, USA.
[2]Institute of Marine Sciences, University of North Carolina at Chapel Hill, Morehead City, North Carolina, USA.

Corresponding author: J. L. Hench, Nicholas School of the Environment, Duke University Marine Laboratory, 135 Marine Lab Road, Beaufort, NC 28516, USA. (jim.hench@duke.edu)

2169-9275/13/10.1002/jgrc.20105

parameterizing the effect of the reef topography on the spatially averaged flow. However, they are less appropriate if coral colonies occupy a significant fraction of the water column or if the region of interest is the near-bottom layer where flow conditions are affected by nearby obstacles.

[4] Previous laboratory and computational studies suggest that flow patterns around isolated coral colonies are qualitatively similar to wakes behind idealized geometries like cylinders and hemispheres. In branching corals, some water passes between branches; however, most water deviates around and even finely branching colonies generate significant wakes [*Kaandorp et al*., 2003; *Chang et al*., 2009]. If corals are sparsely spaced, each colony interacts individually with the free streamflow, but if colonies are more densely spaced, their wakes interact and flow speeds are reduced in a canopy layer that contains solid obstacles. In unsteady flows generated by waves, time-varying pressure gradients force fluid between branches and colonies [*Lowe et al*., 2005, 2007]. In addition to exerting drag forces on the fluid, in unsteady flow there is also an inertial force generated by water accelerating around the coral structure. These forces reduce wave orbital velocities in the layer containing solid obstacles [*Lowe et al*., 2005]. To date, most studies of flow at the scale of a single coral colony have used laboratory and computational approaches with idealized geometries and/or flow conditions [*Kaandorp et al*., 2003; *Lowe et al*., 2005; *Lowe et al*., 2007; *Chang et al*., 2009].

[5] There has been little work that quantifies spatial flow variability under natural flow conditions on real reefs at horizontal scales smaller than 100 m. Thus, there is currently a disconnect between physical oceanographic studies which typically focus on flow at the reef scale and biological questions that often require knowledge of flow conditions at particular points on the reef or the spatial distribution of these smaller-scale flow fields. Here we present the results of field measurements designed to investigate spatial flow patterns on a coral reef in situ, at scales from a single colony to several adjacent colonies (0.1–10 m) under natural flow conditions that vary across a wide range of forcing frequencies. The site of this study, a shallow backreef in Moorea, French Polynesia, is dominated by coral colonies (*Porites* spp.) that vary widely in size and spacing but are roughly hemispherical in shape (referred to hereafter as "bommies"). Questions addressed herein are (1) what are the characteristics of currents and turbulence at the scale of a coral bommie or patch of adjacent bommies?; (2) what are the properties of coral bommie wakes and how do they vary with time as incident flow speeds vary across a range of natural frequencies?; and (3) what are the primary effects of a coral colony on the flow from a dynamical standpoint?

2. Methods

2.1. Field Site

[6] Field measurements were made during January and February 2010, the austral summer, on a shallow backreef on the north shore of Moorea, French Polynesia (17°28.9'S; 149°50.3'W; Figure 1a). The backreef is 1–3 m in depth, and the substrate is largely flat coral pavement populated with colonies of *Porites*, *Montipora*, and *Pocillopora* spp. that vary in size [*Edmunds et al*., 2010]. Many colonies occupy a significant fraction of the water column (typically 30%–90%), particularly massive *Porites* spp. (Figure 1b). Colony spacing is variable, but in general bommies are spaced more densely near the reef crest and further apart toward the interior of the lagoon.

[7] Flow within the lagoon during the austral summer is largely forced by long period, remotely generated swell breaking at the reef crest. Astronomical tides in the system are small (ca. 0.1 m amplitude) due to Moorea's proximity to South Pacific M_2 and K_1 tidal amphidromes [*Hench et al*., 2008]; thus, water levels and currents are not dominated by tidal modulation as they are at many other reef sites [e.g., *Callaghan et al*., 2006]. The primary input of momentum is from waves (and wave groups) breaking at the reef crest which generates radiation stress gradients and water level setup that drives a nearly unidirectional flow across the backreef [*Hench et al*., 2008]. Most of the wave energy is dissipated in breaking. Although velocity fluctuations at wave and wave group frequencies were observed at our backreef site, the mean cross-reef flow direction never reversed. The depth-averaged momentum budget over most of the backreef is well approximated by a simple balance between the cross-reef pressure gradient force and quadratic drag [*Rosman and Hench*, 2011]. After passing over the backreef, water returns to the ocean via several 30–50 m deep reef passes. Flow on the backreef thus varies in concert with the wave forcing from remote swell events that typically span several days [*Hench et al*., 2008].

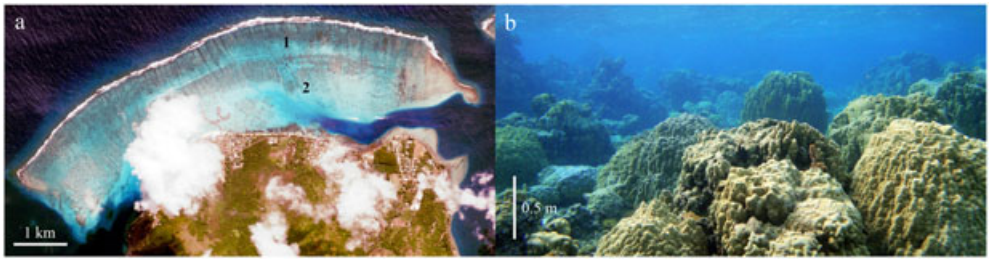

Figure 1. (a) Aerial photograph of backreef field site on north shore of Moorea, French Polynesia, showing locations of velocity measurements, and (b) underwater photograph of site used for two-dimensional spatial mapping measurements over complex topography. Station 1 was the site of the complex bottom topography and 5 year long-term measurements. The spatially resolved and 4 day intensive measurements were made at Station 2.

2.2. Spatial Structure of the Wake Behind a Single Coral Bommie

[8] A single massive colony of *Porites rus* was selected for its approximately hemispherical shape (diameter 1.6 m, height 0.85 m) and location on a flat, open area of the back-reef (mean water depth 2.5 m). The coral colony morphology was typical for *Porites rus*, with a solid interior and a surface covered with 1–5 cm high branches. Velocity measurements were made in the wake in a plane perpendicular to the incident flow (*y*-*z*) using a vertical array of acoustic Doppler velocimeters (ADVs) mounted on a horizontally sliding traverse (Figure 2). The array consisted of seven ADVs with cabled probes mounted on a rigid aluminum frame and arranged with alternating transmit frequencies (6 MHz Nortek Vector and 10 MHz Nortek Vectrino^{+}) to reduce acoustic interference between adjacent instruments. The 6 MHz ADVs ran in self-contained mode and the 10 MHz ADVs were cabled to a computer and DC power supply in a boat anchored nearby. ADV probes were oriented into the flow, aligned with their probes $< 2^{\circ}$ from level, and recorded data continuously at 16 Hz.

[9] At each position in the *y*-*z* measurement plane, data were collected by the seven ADVs for 4 min. Divers repositioned the vertical array by sliding it systematically across the traverse to map out a (*y*-*z*) velocity section. Measurement spacing was 0.2 m in both the horizontal and vertical directions. Velocity *y*-*z* sections were measured at four distances behind the bommie (0.4, 0.8, 1.6, and 2.4 m), corresponding to $x/L = 0.25$, 0.5, 1.0, and 1.5 bommie diameters (L) downstream (Figure 2). Measurements for each *y*-*z* slice took 2 h; thus, the four sections were collected over an 8 h period. Spatial resolution and measurement durations were limited by logistical considerations including diver endurance and daylight boat operations. The 4 min sampling period was selected to capture multiple realizations of the largest turbulent length scales, while still permitting sufficient time to complete the measurements in a single field day to minimize variations in incident flow conditions.

[10] During all measurements an additional stationary 6 MHz ADV was deployed away from obstacles 2.0 m upstream from the bommie and 1.0 m above bottom. Measurements from this instrument were used to normalize measurements from the downstream array to account for temporal flow variations. The mean upstream flow speed during the measurement period was 0.15 m s^{-1}, and the maximum and minimum 4 min averaged flow speeds were 0.23 and 0.08 m s^{-1}, respectively. Although this range of flow speeds could cause some variation in wake length, the measurements were sufficient to resolve the major features of the wake structure.

2.3. Spatial Structure of the Flow Around Complex Reef Patches

[11] Spatial measurements were repeated behind a morphologically complex patch of reef that was the same distance from the reef crest and in the same water depth as the single bommie described above. Measurements were made in a single 7.2 m long *y*-*z* section perpendicular to the flow direction. The same ADV array, horizontal and vertical resolution, and sampling scheme were used as for the single bommie measurements. A single upstream ADV was mounted away from obstacles at 1 m above bottom, and measurements from this instrument were used to normalize measurements from the downstream array.

[12] A second set of measurements was made over a topographically complex 3 m by 10 m area of reef. The topography of this reef patch was too complex to permit deployment of the vertical or horizontal ADV arrays described above. Instead, a single 6 MHz ADV was deployed with the sensor head mounted on a small portable stand with the sampling volume 0.25 m above the substrate. The sensor was moved systematically over the reef in an

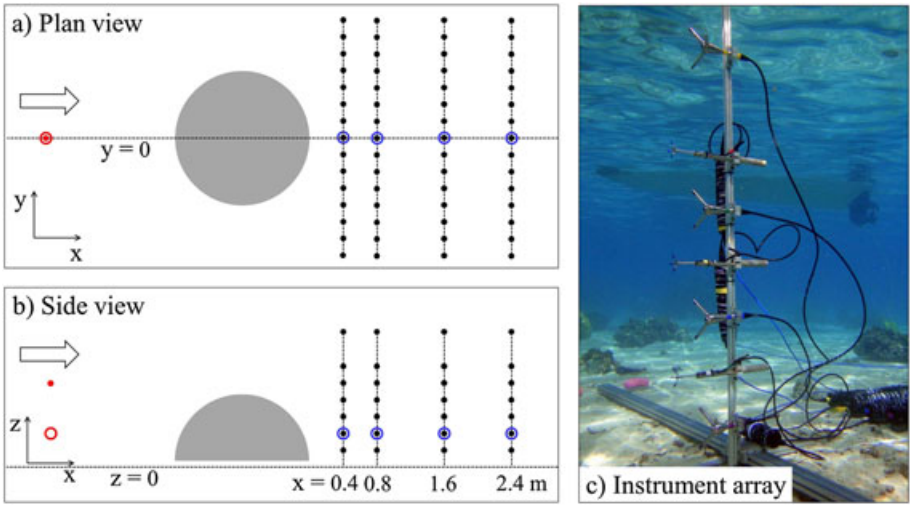

Figure 2. Locations of velocity measurements in the wake of a single coral colony. Small filled circles indicate positions of ADV velocity measurements in the (a) *x*-*y* and (b) *x*-*z* planes for the spatial mapping experiments. Open arrows indicate flow direction. Open circles are locations of ADVs for 3 day time series measurements. Data were normalized by an upstream measurement (shown in red symbols). (c) Underwater photo of instrument array used for spatial mapping; the ADVs were translated across the *y*-*z* section using a sliding traverse.

along-reef (y) transect with 0.25 m spacing between sample locations. An identically configured stationary ADV was deployed on one edge of the box and measurements from this instrument were used to normalize the data from the roving ADV to account for temporal variations in flow.

[13] Reef topography for the two-dimensional reef patch was determined using a set of pressure sensors (RBR, DR-1050). The pressure sensors sampled at 1 Hz with ± 0.005 m accuracy and <0.0001 m resolution. The sensors were moved systematically along four along-reef (y) transects, stopping for 30 s at each location. The along-reef (y) spacing between measurements was 0.25 m and the across-reef (x) spacing between transects was 0.5 m. The elevations of the reef substrate were computed by averaging pressure measurements over 30 s blocks and subtracting values recorded at atmospheric pressure from each sensor to obtain pressure relative to a common zero reference value.

2.4. Temporal Variability of the Wake Behind a Single Coral Bommie

[14] To investigate the temporal variability of bommie wake structure, a further set of measurements was made with a horizontal array of ADVs deployed along the streamwise centerline of the colony described above. Five 6 MHz ADVs were deployed upward-looking in fixed locations (0.4, 0.8, 1.6, and 2.4 m downstream and 1.0 m upstream) on a rigid, low profile, aluminum rail anchored to the seafloor (Figures 2a and 2b). The ADV sample volumes were 0.25 m above bottom. The array was deployed for approximately 4 days and ADVs recorded continuously at 16 Hz.

2.5. Seasonal Variability in Incident Flow

[15] To better understand how seasonal differences in incident flow affect colony-scale hydrodynamic processes, a single upward-looking acoustic Doppler current profiler (2 MHz Nortek AquaDopp) was deployed during the 5 year period from 1 Januarry 2007 to 31 December 2011. The instrument was mounted on the seafloor at the western edge of the complex two-dimensional reef flat patch described above. The profiler recorded velocities at 2 Hz in a 2048 sample burst every 2 h. For the analysis, we used velocities from one 0.75 m bin, centered 0.6 m above bottom.

2.6. Data Analyses

[16] All ADV velocity (u,v,w) data were rotated into a coordinate system with positive x toward the shoreline (approximately southward), y along-reef (approximately eastward), and z upward (Figure 2). Velocity data were despiked and screened for low beam correlations and missing data (~1%) were filled by interpolation. To account for temporal variability in the incident flow while the spatially resolved measurements were made, traversing ADV velocities were normalized by dividing by time-averaged data from the upstream ADV (designated as U, V, W). Time averages were computed over 4 min intervals for spatial mapping measurements and 1 min intervals for time series measurements.

[17] Power spectra were computed from 16 Hz velocity measurements using Welch's averaged periodogram method [e.g., *Emery and Thomson*, 2001] with a Hann window. For spatial mapping measurements, spectra for 7 × 1 min segments with 50% overlap were averaged to determine the spectrum for each spatial position. For time series measurements, spectra were computed for 30 min intervals by averaging 7 × 5 min segments with 50% overlap. Turbulent dissipation rates (ε) were calculated from fits to the inertial subrange of a one-dimensional spectrum of velocity fluctuations [*Pope*, 2000; *Shaw et al*., 2001]. The streamwise velocity spectrum was used to estimate dissipation for spatial mapping measurements and the vertical velocity spectrum was used for time series measurements. In each case, this corresponded to the direction with the lowest instrument noise floor (i.e., parallel with the transmitted acoustic beam). The fit was performed in frequency space using a frozen turbulence assumption, such that,

$$S(f) = \frac{18}{55}\alpha\left(\frac{\bar{u}}{2\pi}\right)^{2/3}\varepsilon^{2/3}f^{-5/3} \quad (1)$$

where S is power spectral density as a function of frequency f, $\bar{u}$ is the local time-averaged flow speed, $\alpha = \alpha_1 = 1.5$ for the streamwise (u) spectrum and $\alpha = (4/3)\,\alpha_1 = 2$ for the vertical (w) spectrum [*Pope*, 2000]. All data segments where the velocity standard deviation $\sigma_u > 2|\bar{u}|$ were rejected because the frozen turbulence assumption was inappropriate [e.g., *Gerbi et al*., 2008]; this criterion primarily affected points within recirculation zones immediately behind coral colonies. Dissipation was also not computed for data segments where the inertial subrange fit had $r^2 < 0.25$ or when mean flows were less than 0.025 m s^{-1}.

[18] Reynolds stresses were computed from the integral of the cospectrum above the wave band ($f > 0.08$ Hz). While this likely underestimates Reynolds stresses, we can be certain that these estimates were not biased by correlations between orthogonal components (x-y, x-z) of the slowly varying flow.

3. Results

3.1. Spatial Structure of the Wake Behind a Single Coral Bommie

[19] Velocities behind the single isolated coral bommie were significantly reduced relative to upstream and dissipation was elevated, indicating a strong turbulent wake (Figures 3 and 4). Across-reef velocities were sharply reduced immediately behind the bommie, within 0.25 bommie diameters, and flow converged around the sides (Figure 3a). Near the bommie center, flow direction was reversed and directed offshore, suggesting that flow separated around the bommie edges, creating a recirculation zone. These observations are consistent with numerical simulations and laboratory measurements of flow separation behind a hemisphere at similar Reynolds numbers [*Savory and Toy*, 1986; *Manhart*, 1998]. *Chamberlain and Graus* [1975] did not observe a recirculation zone behind a branching colony in a flume study at similar colony Reynolds numbers to our measurements; however, the methods they used to measure flow speed did not resolve flow direction, limiting their ability to identify a flow reversal. More recent high-resolution flume measurements [*Chang et al*., 2009] and numerical simulations [J. Rosman, unpublished] of flow through a fine branching morphology of *Stylophora pistillata* show a weak recirculation zone; however, in these

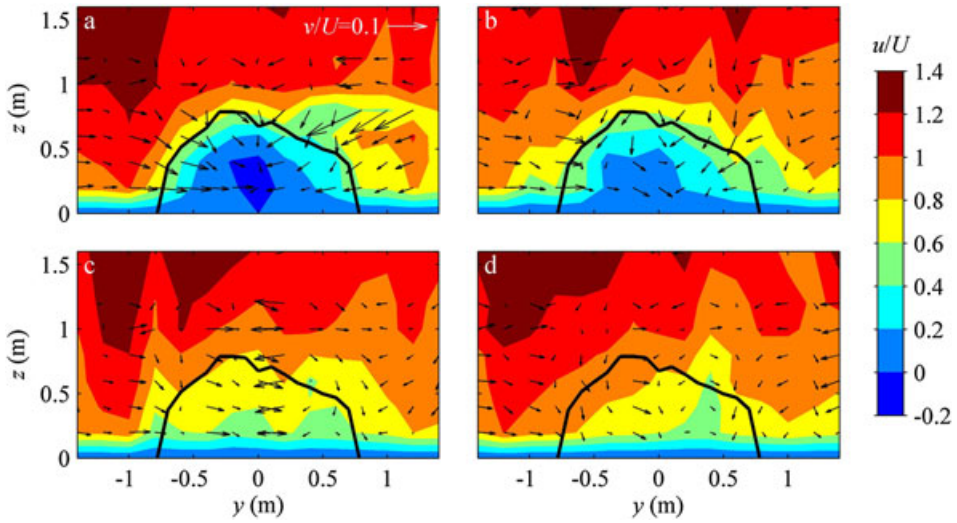

Figure 3. Velocity sections (*y*-*z*) in the wake of a single coral colony at four distances downstream: (a) 0.4 m, (b) 0.8 m, (c) 1.6 m, (d) 2.4 m. Velocities are time averages over 4 min intervals and are normalized by upstream values. Color contours are cross-reef velocities (perpendicular to page). Vectors represent in-plane velocity components. The solid black line indicates the outline of the top edge of the colony.

studies water was able to pass through the colony as well as around it and colony Reynolds numbers were a factor of 10–50 smaller than for the field measurements described here.

[20] Above the top of the bommie, flow velocities were relatively strong; thus, there was a shear layer ($\partial u/\partial z$) between the "dead-zone" in the lower water column and the fast-moving fluid in the upper water column (see also Figure 5). Similarly, there was strong lateral shear ($\partial u/\partial y$) between fast moving fluid that passed around the sides of the bommie and slow-moving fluid immediately behind the bommie. These shear regions coincide with peaks in Reynolds stresses; there was a peak in $\overline{u'w'}$ at the top of the wake and a peak in $\overline{u'v'}$ on the sides of the wake (Figure 5). The peak in flow speed to the right of the bommie at $z = 0.6$ m in Figure 3a is thought to be due to flow acceleration over a small (~0.4 m high) bommie that was adjacent to the large bommie and slightly upstream.

[21] Although at low wave numbers, turbulence was anisotropic as indicated by the nonzero Reynolds stresses, the inertial subrange turbulence was isotropic, enabling dissipation rates to be calculated from fits to the inertial subrange. Dissipation rates were elevated in the bommie wake (Figures 4, 5c, and 5f), and dissipation rate was a maximum about 0.5 diameters (L) from the back of the bommie

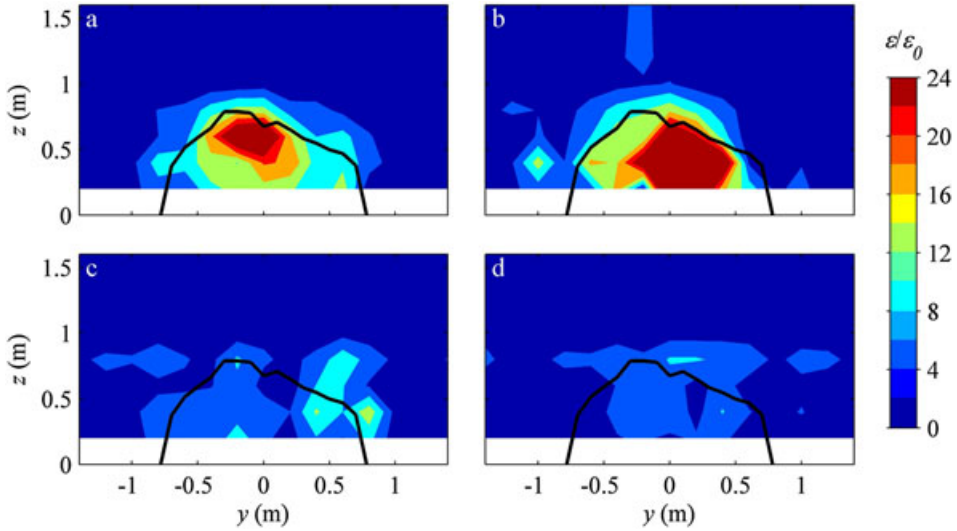

Figure 4. Spatial structure of turbulent dissipation rate in the wake of the coral colony across four *y*-*z* sections at different distances downstream: (a) 0.4 m, (b) 0.8 m, (c) 1.6 m, (d) 2.4 m. The solid black line indicates the top edge of the colony. All turbulent dissipation rates (ε) were normalized by the upstream dissipation rate (ε_0).

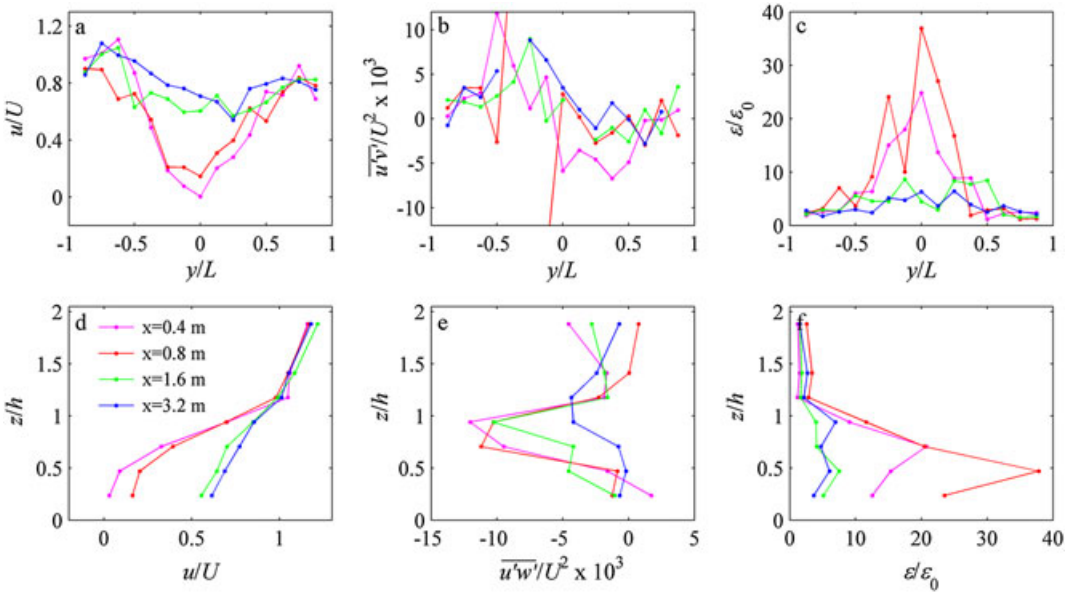

Figure 5. (a, d) Velocities, (b, e) Reynolds stresses, and (c, f) turbulent dissipation rates at four distances downstream (x) from the back of the coral colony. The top row shows horizontal profiles of the average of measurements at $z = 0.4$, 0.6, 0.8 m above bottom. The bottom row shows vertical profiles of the average of measurements directly behind the colony ($y = -0.4$, -0.2, 0, 0.2, 0.4 m). Elevations above seafloor are normalized by the bommie height (h); other quantities have been normalized by upstream values (U, ε_0) at 1 m above bottom.

($x/L = 0.5$). Spatial patterns in dissipation rate and shear were not aligned (Figures 3 and 4). While shear production was greatest around the periphery of the wake and small in the wake interior, dissipation rates were also elevated in the recirculation zone immediately behind the bommie, suggesting that there was not a local balance between shear production and dissipation of turbulent kinetic energy and that transport terms in the turbulent kinetic energy budget were likely significant. Observed patterns in production and dissipation are consistent with advection of turbulence from high shear zones around the wake periphery to lower shear zones in the wake interior by the flow around the bommie.

[22] With increasing distance downstream from the bommie (Figures 3 and 4) the wake attenuates. At a distance of two bommie diameters downstream ($x/L = 2$), a small velocity deficit and slight elevation in dissipation rate are still evident (Figures 3d, 4d, 5c, and 5f).

3.2. Spatial Structure of the Flow Around Complex Reef Patches

[23] The spatial structure of the wake behind the complex reef patch had many of the same characteristics as the single bommie wake (Figure 6). Immediately behind the reef patch, there was a recirculation zone in which flow was reversed and directed upstream (offshore). Velocities had a downward component as flow that had passed over the topography joined the recirculating eddy and wake. There was a strong shear layer between the slow-moving fluid behind the topography and the fast-moving fluid above. Turbulent dissipation rates were elevated in the shear layer, but maximum dissipation rates occurred lower in the water column, again suggesting significant downward advective transport of turbulence. Above the topography and in the channel between the two sections of topography, flow speeds were greater than upstream, likely due to flow being accelerated over and between the topography, forming a near-bottom jet in the latter case.

[24] Measurements of flow over the complex two-dimensional reef patch illustrate some of the flow features that might be expected when bommies are spaced closely enough that flow sheltering and wake-wake interactions occur (Figure 7). Time-averaged flow speeds and velocity variances were generally higher in the water column, on the tops of bommies, than lower in the water column and on the adjacent seafloor. However, flow accelerated between bommies (e.g., Figure 7; sixth arrow from the left) in areas not sheltered by upstream obstacles. Dead zones were observed low in the water column, behind bommies (e.g., Figure 7; third, fourth, and tenth arrows from right). Principal axes of variance ellipses tended to align with topography and channels between upstream obstacles, consistent with expectations that flow would be steered by the small-scale topography.

3.3. Temporal Variability of the Wake Behind a Single Coral Bommie

[25] The 4 day time series of velocity measurements behind the bommie were used to investigate the temporal variability in wake structure. The measurements spanned a large swell event that increased currents across the backreef; ambient 30 min averaged flow speeds at the site ranged from 0.10 to 0.22 m s^{-1} over the 4 day period (Figure 8a). Temporal patterns in flow speeds behind the bommie were highly correlated with those upstream. Immediately behind the bommie ($x/L = 0.25$), flow was reversed in direction and the strength of the recirculation zone increased as incident flow speed increased. At all other measurement positions, flow direction was the same as for the incident flow. At $x/L = 1.5$,

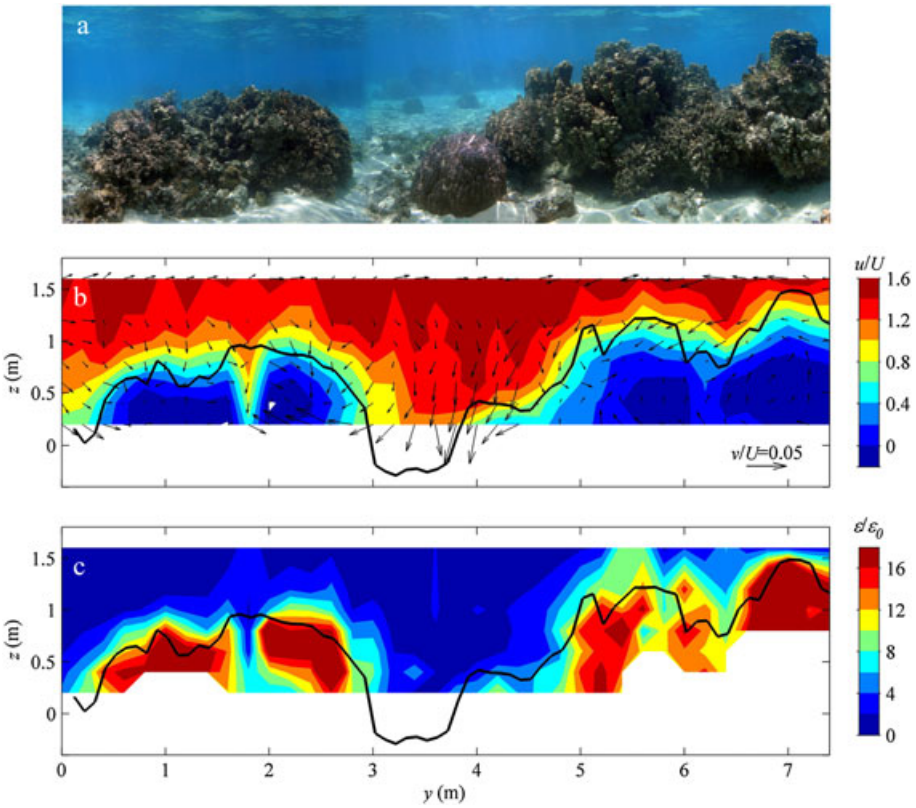

Figure 6. Measurements behind complex reef topography: (a) photo mosaic of reef; (b) normalized velocities in the wake with contours representing across-shore (streamwise) components and vectors representing in-plane components; and (c) normalized turbulent dissipation rates. The solid black line indicates the top edge of the reef. White areas in Figure 6c are points where the assumptions in the dissipation rate calculations were invalid.

a velocity deficit was still evident for all incident flow speeds. Turbulent dissipation rates (Figure 8b) were also strongly modulated by the incident forcing, varying by over an order of magnitude at each location as incident flow speed varied. Dissipation rates were greatest at the two measurement positions closest to the bommie ($x/L = 0.25,\ 0.5$) and were a factor of two greater than values upstream at $x/L = 1.5$.

[26] To investigate the relationship between recirculation zone strength, wake length, and incident flow speed, ADV data were binned according to incident flow speed and bin averages were computed (Figure 9). At slow incident velocities, the flow immediately behind the bommie was nearly stagnant and flow speed gradually increased with distance downstream. For incident flows greater than $0.1\ \mathrm{m\,s^{-1}}$, a recirculation cell formed behind the bommie and near-bottom mean velocities were directed upstream (offshore; Figure 9a).

[27] Downstream from the recirculation zone, the flow reattached to the bottom and flow speeds increased with downstream distance. The point of flow reattachment (dividing streamline) moved downstream as incident flow speed increased, from $x/L = 0.25$ for $U < 0.1\ \mathrm{m\,s^{-1}}$ ($UL/\nu = 1.6 \times 10^5$) to $x/L = 0.5$ for $U > 0.3\ \mathrm{m\,s^{-1}}$ ($UL/\nu > 4.8 \times 10^5$) (Figure 9b). The distance to reestablishment of the upstream flow increased with increasing flow speed; for example, for incident flow speeds $> 0.30\ \mathrm{m\,s^{-1}}$, this distance was 50% greater than for incident flow speeds of 0.10–$0.20\ \mathrm{m\,s^{-1}}$. At flow speeds greater than $0.30\ \mathrm{m\,s^{-1}}$, the shape of the wake and strength of the recirculation zone

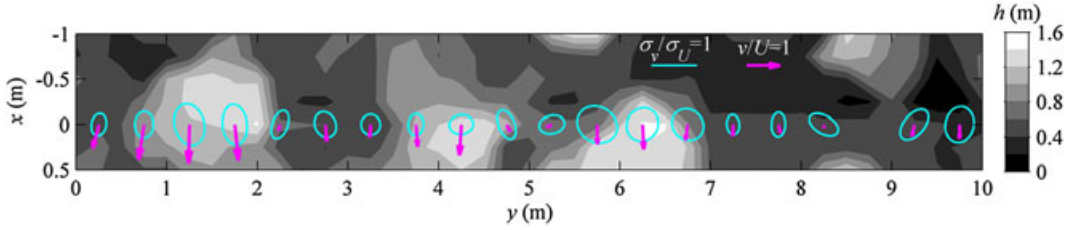

Figure 7. Transect of velocities across a complex bottom at 20 cm above the substrate. Gray shaded contours are the bottom topography height (h) above a fixed datum, magenta arrays are 3 min–averaged velocities and variance ellipses are indicated in cyan.

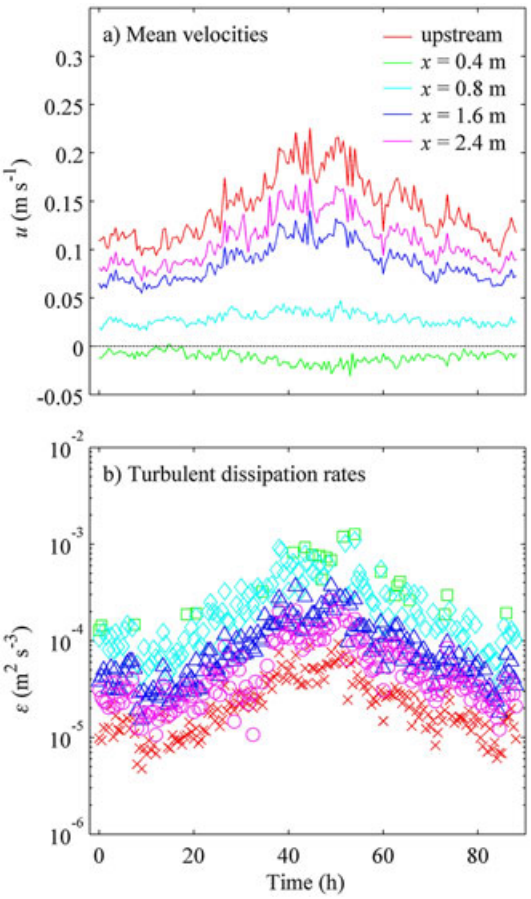

Figure 8. Time series of (a) across-reef 30 min–averaged velocities and (b) turbulent dissipation rates at 0.25 m above bottom, upstream of the coral colony and at four distances downstream along the centerline of the colony wake (Figure 2). Negative velocity is flow toward the reef crest and indicates flow reversal.

relative to incident flow appeared to be constant (invariant with incident flow speed; Figures 9b and 9d). The largest dissipation rates occurred immediately behind the bommie and greater incident velocities resulted in larger dissipation rates (Figures 9c and 9d).

[28] Velocities downstream of the bommie are affected by the bommie wake and the redevelopment of the bottom boundary layer. Here we define an effective wake length (L) to be the distance downstream of the bommie at which the upstream flow condition is reestablished. To estimate effective wake length, velocity data for each incident flow speed in Figure 9b were fit with a function representing the decay distance of the velocity deficit in the wake relative to the upstream velocity:

$$u/U = 1 - \exp[-a(x/L) + b] \tag{2}$$

where a and b are fitting parameters. All fits had r^2 values > 0.99. The wake length was defined as the distance downstream from the bommie at which the velocity returned to 99% of the upstream velocity. The resulting wake lengths (Figure 10) were about three bommie diameters at the slowest flow speeds and five diameters at the fastest flow speed, which appeared to be the upper limit in the data. This suggests that for incident flow speeds $>0.3\ \mathrm{m\,s^{-1}}$, effective wake length was not Reynolds number dependent. Reynolds numbers were large enough that the wake was fully turbulent during the entire observational period. It is unclear why the wake length appears to increase with Reynolds number for $u < 0.3\ \mathrm{m\,s^{-1}}$, although it is possible that redevelopment of the bottom boundary layer influenced the estimates of effective wake length.

[29] To further investigate the partitioning of energy between velocity variations at different frequencies, we computed spectra from 4 day velocity time series (Figure 11). At all stations, there was a peak in the power spectrum between 12 and 20 s with similar energy at all measurement positions. This peak represents velocity variations due to individual waves and comprises about 20% of the total velocity variance (Figures 11c and 11f). At frequencies higher than this peak, there was increased energy at all stations downstream from the bommie relative to upstream (Figure 11a).

[30] The contributions to the total variance from low ($0.01 < f < 0.05$ Hz), medium or wave band ($0.05 < f < 0.1$ Hz), and high ($0.1 < f < 2$ Hz) frequency velocity fluctuations were computed by integrating those regions of the spectrum:

$$\mathrm{var}_{f_1 f_2}(u) = \int_{f_1}^{f_2} S_{uu}(f)\,df \tag{3}$$

The integral was evaluated numerically using a trapezoid rule. A similar set of calculations was done for the vertical velocity spectra.

[31] Low-frequency variations accounted for most (60%–80%) of the total variance at each position and wave-band and high-frequency variations each accounted for 10%–30% of the total variance. Spatial patterns in low-frequency u variations (Figure 11b) were similar to patterns in the mean currents (Figure 10b); the velocity variance was smallest closest to the bommie and increased with downstream distance, presumably returning to the upstream value far downstream, beyond the region of influence of the bommie (and our measurements). This variance is primarily due to variations in the incident flow speed. Velocity variations in the wave band were relatively independent of position, suggesting that flow patterns around the bommie at frequencies in the wave band differed from those at lower frequencies. The velocity variance in the wave band was $\sim 8 \times 10^{-4}\ \mathrm{m^2\,s^{-2}}$ (Figure 11a); therefore, the standard deviation of velocity variations in the wave band was about $0.03\ \mathrm{m\,s^{-1}}$. The Keulegan-Carpenter number (KC) representing the ratio of water excursion to object diameter was $uT/L \sim 0.03 \times 20 / 1.6 = 0.4$. Wake-like flow patterns were therefore observed downstream of the bommie when water excursion was greater then bommie diameter ($KC > 1$, $f < 0.02$ Hz), while substantially less effect of the bommie was seen when water excursions were less than bommie diameter ($KC > 1$, $f > 0.02$ Hz).

[32] The spatial patterns in the variance of high-frequency fluctuations (Figures 11b and 11d) were similar to those for dissipation rate (Figure 10d); high-frequency fluctuations

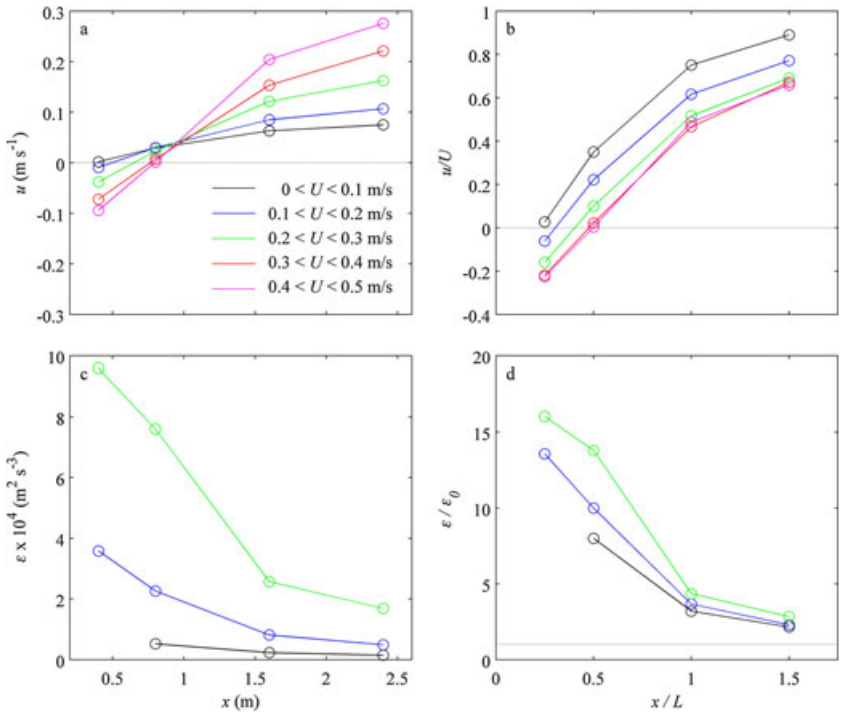

Figure 9. Spatial structure of the wake behind the coral colony for different upstream velocities U: (a) mean velocities; (b) velocities normalized by upstream values; (c) dissipation rates; and (d) dissipation normalized by upstream values.

were most energetic closest to the bommie and decreased in energy with downstream distance likely due to vortices shed from the bommie and associated turbulence. High-frequency variations contributed most to the total variance immediately downstream of the bommie. Low- and medium-frequency fluctuations in w followed a similar pattern to high-frequency fluctuations because the majority of the vertical variance came from redistribution of mean flow kinetic energy from the streamwise component to the vertical component as water deviated over the bommie.

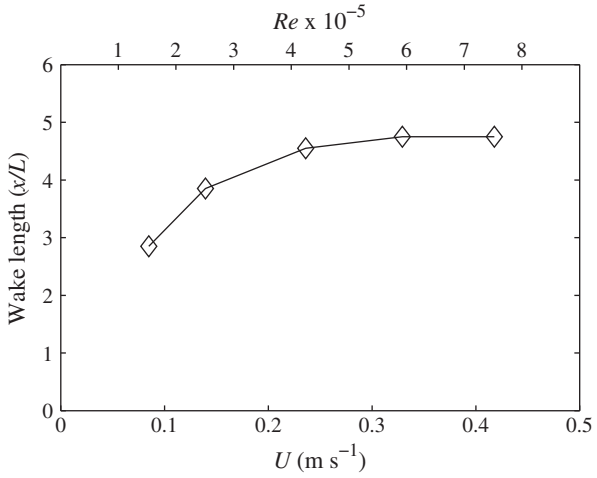

Figure 10. Coral colony wake length (distance downstream required to return to 99% of upstream flow) as a function of incident flow speed and Reynolds number based on colony diameter. Effective wake lengths were computed from data in Figure 7b using equation (2).

4. Discussion

[33] While the wake behind the coral colony persisted throughout the observation period, its characteristics varied with time as incident flow conditions varied. In general, larger incident flow speeds resulted in a stronger recirculation behind the colony and a longer, more turbulent wake. However, the extent to which variations in the incident flow were damped behind the colony depended on their frequency. Low-frequency (<0.03 Hz) variations were strongly damped behind the colony while wave-band (0.05–0.1 Hz) variations were similar upstream and downstream. We now consider the dynamics of the interaction between the incident flow and the coral colony and the implications for the larger-scale flow and biological processes on reefs.

4.1. Dynamics of the Interaction Between the Incident Flow and a Single Coral Colony

[34] In this section, we consider the forces exerted on the water by a single colony and the mechanisms for energy removal from the mean flow. As time-varying flow deviates around a coral's structure, pressure gradients are established due to flow separation and acceleration around the colony. The net force on a solid obstacle arising from these pressure gradients is typically described as the sum of two components, a drag force (F_D) and an inertial force (F_I). The drag force represents the integral around the object surface of the pressure due to separation of the steady flow. The inertial force represents the surface integral of the pressure generated acceleration of fluid around the object [*Dean and*

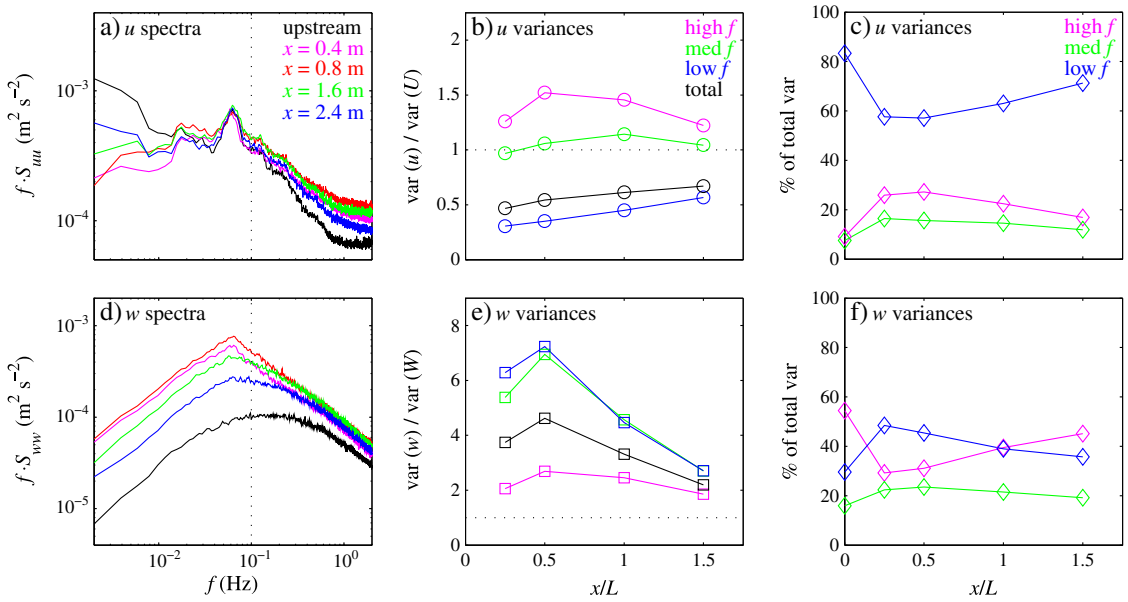

Figure 11. Velocity spectra and variances in the wake of the coral colony. Spectra are in variance preserving form. Vertical lines in panels (a, d) indicate the cutoff between high- and low-frequency bands used to compute variances in panels (a, c) and 11e. Horizontal lines in panels (b, e) are the normalized upstream variences (unity, by definition).

Dalrymple, 1991]. Forces equal in magnitude but opposite in direction are exerted by the coral colony on the fluid.

[35] Form drag is typically parameterized using a quadratic drag law [e.g., *Kundu*, 1990],

$$F_D = \frac{1}{2}\rho c_d A U^2 \tag{4}$$

where c_d is the drag coefficient which is $O(1)$, A is the obstacle frontal area ($A = \frac{1}{2}\pi(\frac{L}{2})^2$ for a hemisphere with diameter L), and U is the incident flow speed.

[36] In laboratory experiments of flow over hemispherical domes in turbulent boundary layers, *Taniguchi et al.* [1982] and *Meroney et al.* [2002] observed $c_d \sim 0.3$ (range 0.2–0.4) for similar Reynolds numbers to our field observations. The reference velocity for the drag parameterization was the free stream velocity in *Taniguchi et al.* [1982] and the incident flow speed at the top of the hemisphere in *Meroney et al.* [2002]. The two velocities are approximately equal in these previous studies and for our measurements; therefore, we used $c_d = 0.3$ for all our analyses. If the incident flow velocity is decomposed into a mean and a series of sinusoids, then the drag force is in phase with velocity variations at any given frequency; therefore, work is done by the drag force and it results in a conversion of energy from the incident flow to turbulence.

[37] The inertial force exerted by an accelerating fluid on a solid obstacle (and by the obstacle back on the fluid) is the sum of a component due to the pressure gradient responsible for accelerating the ambient flow (F_{I1}), also termed the virtual buoyancy force, and a component due to the pressure gradient generated as the fluid accelerates around the obstacle (F_{I2}), also termed the added mass force [*Dean and Dalrymple*, 1991]. F_{I1} would exist in the fluid in the absence of the obstacle; therefore, F_{I2} is the net additional force exerted by the obstacle on the fluid. The inertial force can be expressed

$$F_I = F_{I1} + F_{I2} = \rho(1 + k_m)\mathbf{V}\frac{\partial U}{\partial t} \tag{5}$$

[38] Here k_m is an $O(1)$ added mass coefficient that depends on the obstacle shape, $\mathbf{V}$ is the obstacle volume, equal to $\pi L^3/12$ for a hemisphere, and $\partial U/\partial t$ is the acceleration of the incident flow. For a bluff object, $k_m = 1$ is a reasonable approximation and this value was used here. The inertial force is in phase with acceleration but in quadrature with velocity variations at any given frequency; therefore, it does not result directly in energy loss. Rather it generates a local oscillatory force that opposes the background pressure gradient and thus decreases the amplitude of velocity oscillations locally around a colony without removing energy. If colonies are spaced closely, inertial forces can significantly reduce the amplitude of velocity variations in the colony canopy layer [*Lowe et al.*, 2005]. Implications include reduced mass transfer to corals and other organisms and reduced drag forces leading to less removal of energy from flow variations [*Lowe et al.*, 2007].

[39] To examine the significance of drag and inertial forces on water moving across the backreef, we first computed the forces exerted on the flow by the single hemispherical colony. F_D and F_I were computed from 1 s averaged upstream velocity time series using equations (4) and (5). The means and standard deviations of these forces were then computed over 1 h periods. Because F_I is proportional to acceleration which is very small for the slowly varying (1 h averaged) flow, the only significant force on the current is drag (Figure 12a). The maximum 1 h averaged drag occurred in the middle of the 4 day record when the cross-reef

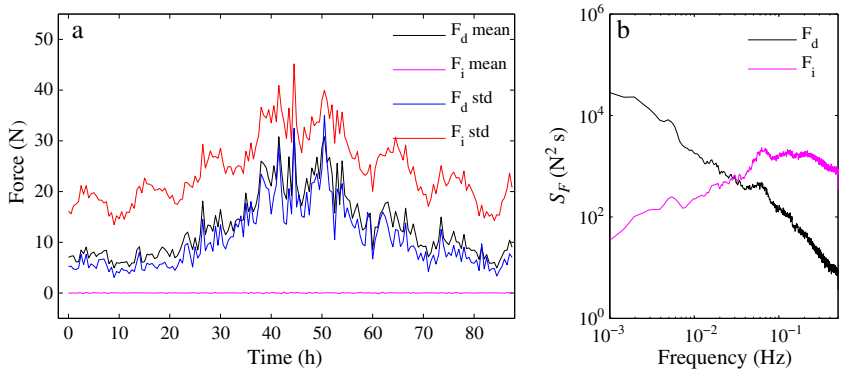

Figure 12. Drag and inertial forces exerted on the water by the coral colony: (a) time series of the 1 h mean and 1 h standard deviations of the forces and (b) average spectra over the complete 4 day record.

flow was largest. However, the standard deviation of the inertial force was always larger than the standard deviation of the drag force, suggesting that the inertial force had important effects on the instantaneous flow.

[40] To examine the relative importance of drag and inertial forces across the range of observed time scales, it is informative to consider their spectra (Figure 12b). At any given frequency, the spectral densities are a measure of force fluctuations at that frequency. Drag is the dominant force on low-frequency (<0.03 Hz) flow variations, but the inertial force is the largest acting on flow variations at higher frequencies (>0.03 Hz), including the wave band (0.05–0.1 Hz).

[41] For a sinusoidal signal, amplitude is proportional to standard deviation. The ratio of standard deviations therefore indicates which force, drag, or inertia has the largest effect on flow variations at a given frequency (ω):

$$\frac{F_{D,\mathrm{std}}}{F_{I,\mathrm{std}}} = \frac{\frac{1}{2}c_d A}{(1+k_m)\mathbf{V}} \frac{\mathrm{std}(U^2)}{\mathrm{std}\left(\frac{\partial U}{\partial t}\right)} \tag{6}$$

[42] Velocity variations were assumed to be sinusoidal in time; that is, $U = \bar{u} + \sqrt{2}U_{\mathrm{std}} \sin\omega t$ where U_{std} is the velocity standard deviation at frequency ω and $\bar{u}$ is the time-averaged (slowly varying) velocity. If $\bar{u} > U_{\mathrm{std}}$, the case for our measurements, equation (6) reduces to $\frac{F_{D,\mathrm{std}}}{F_{I,\mathrm{std}}} \approx \frac{3c_d}{2(1+k_m)} \frac{\bar{u}}{L\omega}$. This is a sort of Keulegan-Carpenter number; the transition from drag-dominated to inertia-dominated regimes occurs when the excursion of water due to the slowly varying flow during the time for one velocity oscillation ($\omega/\bar{u}$) becomes small compared with the obstacle dimension (L). This transition coincides with the frequency above which flow variations downstream of the colony were similar to those upstream (Figure 11).

[43] The drag force does work on the fluid as it moves past the coral colony resulting in the generation of turbulence. This was reflected in elevated dissipation rates we observed downstream of the colony. Expressed in terms of total work per unit time; this is,

$$\frac{\mathrm{work}}{\mathrm{time}} = F_D \cdot U = \frac{1}{2}\rho c_d A U^3 \tag{7}$$

[44] The observed dissipation rate in the wake (at $x/L = 0.5$) was strongly correlated with the work done by the drag force (Figure 13; $r^2 = 0.86$). The slope of this regression (11 m^3) has units of volume and can be thought of as the volume of water within which mean flow kinetic energy is dissipated by turbulence in the wake. The volume integral of ε calculated from the spatially resolved sections (Figure 4), divided by the dissipation rate at $x/L = 0.5$, gave an effective dissipation volume of about 2 m^3. These two estimates agree within an order of magnitude and are physically reasonable based on the observed wake dimensions (Figure 4). The mismatch is most likely a result of uncertainties in the volume integral and the drag coefficient used to compute the work.

4.2. Implications for Reef-Scale Hydrodynamics

[45] Coral colonies can be thought of as having three main effects on bulk flow across reef flats: (1) net drag and inertial forces due to the surface integral of pressure gradients around many individual obstacles, (2) increased mixing due to turbulence production in obstacle wakes, and (3) mechanical dispersion due to persistent spatial flow variations [e.g., *Raupach and Shaw*, 1982; *Nepf*, 1999; *Lowe et al.*, 2005]. In this section, we combine scaling arguments with our observations of colony-scale processes to examine their significance for the reef scale flow.

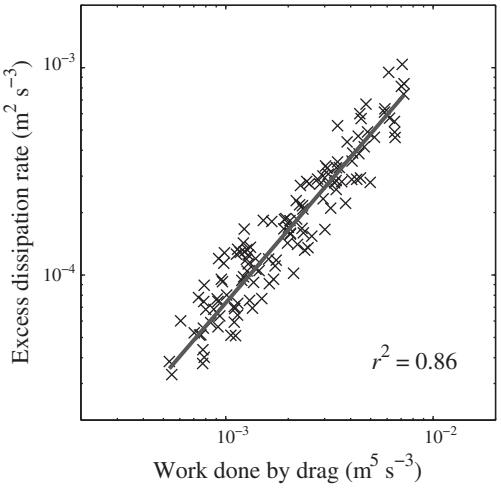

Figure 13. Turbulent dissipation rates in the bommie wake at $x = 0.8$ m, expressed relative to upstream values ($\varepsilon - \varepsilon_0$) versus work done by the drag force.

[46] To evaluate the significance of form drag and inertial forces due to the array of bommies under natural flow conditions on the Moorea backreef, the sizes of these forces were compared with other terms in the spatially averaged momentum budget. First, we consider slowly varying flow for which the inertial force is negligible and the momentum budget is dominated by pressure gradient and drag terms. The drag force (equation 4) per unit fluid mass ($\rho H_{\mathrm{eff}} S^2$) is

$$f_{D1} = \frac{c_d \pi L^2 U^2}{16 H_{\mathrm{eff}} S^2} \tag{8}$$

[47] Here L is bommie diameter, H_{eff} is the effective water depth, the volume of water per unit plan area, S is the spacing (distance between adjacent bommie centers), and U is the incident flow speed at the top of the colony. The depth-averaged drag term in the cross-reef momentum budget is

$$f_{D2} = \frac{C_D U_{\mathrm{davg}}^2}{H_{\mathrm{eff}}} \tag{9}$$

where C_{D} is the bulk drag coefficient and U_{davg} is the depth-averaged velocity. If it is assumed that $U_{\mathrm{davg}} \sim U$, a reasonable assumption if bommies occupy most of the boundary layer, the ratio of f_{D1} estimated from form drag around isolated hemispheres to f_{D2} from the across-reef momentum budget is

$$\frac{f_{D1}}{f_{D2}} = \frac{\pi c_d}{16 C_D} \frac{L^2}{S^2} \tag{10}$$

[48] For the Moorea backreef $C_D = 0.066$–0.1 [*Rosman and Hench*, 2011], a factor of 26–40 times larger than for sand ($C_D \approx 0.0025$). For the net drag due to a hemisphere array (f_{D1}) to match the observed cross-reef drag (f_{D2}; $C_D = 0.066$–0.1) would require $L/S \sim 1$–1.3; that is, bommies would need to be so closely spaced that edges were touching. A more realistic spacing on the Moorea backreef (see Figure 7) is $L/S \sim 0.5$, which yields $f_{D1}/f_{D2} \sim 0.15$–0.22. This scaling result suggests that form drag due to flow around isolated obstacles contributes significantly to overall drag, but we are not able to explain all of the across-reef drag estimated by *Rosman and Hench* [2011] using these arguments. The discrepancy may arise from a combination of factors. For example, drag due to flow around adjacent obstacles can exceed drag due to flow around the same isolated obstacles [*Meroney et al.*, 2002]. Also, if coral colonies are spaced more closely than boundary layer development length scales, the flow may be a series of overlapping wakes and developing boundary layers. If boundary layers are constantly adjusting to changes in surface roughness, the net drag can exceed that for fully developed flow [*Albertson and Parlange*, 1999].

[49] To evaluate the significance of drag and inertial forces for higher-frequency flow variations, we consider their sizes relative to variations in the acceleration term in the spatially averaged momentum budget. Below we compare the standard deviations of these terms because this is the same as comparing their amplitudes and therefore gives an indication of how large an effect each term has on velocity fluctuations at a given frequency. The ratio of the drag term to the acceleration term is

$$\frac{f_{D,\mathrm{std}}}{(\partial U/\partial t)} = \frac{\pi c_d}{8} \frac{L^2}{S^2} \frac{\bar{u}}{\omega H_{\mathrm{eff}}} \tag{11}$$

[50] The ratio of the inertial force term to the acceleration term is

$$\frac{f_{I,\mathrm{std}}}{(\partial U/\partial t)} = k_m \phi \tag{12}$$

where ϕ is the solid volume fraction, equal to the volume of solid obstacles divided by the total (fluid plus solid) volume. From equation (12), the inertial force only affects velocity fluctuations at a given point on the reef if solid obstacles occupy a significant volume compared with the fluid. The ratio of this term to the acceleration does not depend on attributes of the flow. In contrast, drag is more significant for low-frequency variations and less significant for higher-frequency variations. Although for high-frequency variations, drag is small compared with other terms in the momentum budget, it results in a conversion of energy from mean flow kinetic energy to turbulence. When this effect is integrated across the reef width, it may result in a significant loss of energy from flow variations at higher frequencies from the reef's offshore edge to its inshore edge.

[51] The presence of obstacles in the flow also affects vertical and horizontal turbulent mixing and thus turbulent shear stresses. Our results illustrated that the turbulent dissipation rate in a volume downstream of a coral colony is closely related to the work done by the drag force (Figure 13). For the single colony, assuming all of the energy lost from the incident flow is converted to turbulence, the net energy converted from mean kinetic energy to turbulent kinetic energy per unit time is given by equation (7). In a spatially averaged sense, the wake production of turbulent kinetic energy per unit volume is therefore

$$P_{wake} = \frac{\frac{1}{2} c_d A U^3}{S^2 H_{\mathrm{eff}}} = \frac{U^3 L^2}{16 S^2 H_{\mathrm{eff}}} \tag{13}$$

where we have substituted $A = \frac{1}{2}\pi\left(\frac{L}{2}\right)^2$ and $c_{\mathrm{d}} = 0.3$. For fully developed boundary layer flow over a sand bottom with $u_* \sim 0.05U$, velocity shear is $u_*/\kappa z \sim 0.12U/z$ and stress is $u_*^2 \sim 0.0025U^2$. Thus, production is $\sim 0.0003U^3/z$ and volume-averaged production, estimated by integrating a logarithmic velocity profile over the water depth is $\sim 0.0003U^3 \ln(H/z_0)/H$. The ratio of volume-averaged turbulence production due to bommie wakes to that in a boundary layer over sand is therefore

$$\frac{P_{\mathrm{wake}}}{P_{\mathrm{sand}}} \sim \frac{200}{\ln {}^{H}/_{z_0}} \frac{L^2}{S^2} \sim 54 \frac{L^2}{S^2} \tag{14}$$

where $z_0 \sim 0.05$ m was assumed for sand. These scaling arguments suggest that if $L/S = O(1)$, wake production associated with flow around large obstacles contributes significantly to net conversion of mean flow kinetic energy to turbulent kinetic energy on the reef.

[52] Here we have assumed that the reef can be approximated as a series of hemispheres with noninteracting wakes.

In general, reefs geometries vary across a range of spatial scales and perhaps can be decomposed into series of simple objects (e.g., hemispheres, cylinders, sine waves) with different dimensions. Depending on their spacing the level of interaction between these elements could vary, altering the spatially averaged forces and wake production of turbulence, and this merits further investigation.

4.3. Variation in Spatial Flow Patterns at Seasonal Time Scales

[53] Above we addressed small-scale flow variability over time scales up to days; however, on many coral reefs, the remotely generated forcing that drives circulation across the reef can vary over seasonal time scales. At our study site on the north shore of Moorea, much of the forcing arises from exposure to remote swell generated by storm systems in the North Pacific [see *Bromirski et al*., 2005]. Large south swell from the Southern Ocean also impinges on the island of Moorea, but our north facing field site is largely sheltered from this activity. To better understand variability at these time scales, currents from a nearly continuous 5 year record were used to investigate variation in across-reef flow and predict differences in wake characteristics between seasons (Figure 14). During the austral winter, currents on the backreef are typically small (~0.05–0.1 m s^{-1}), while in the austral summer when swells from remote storms break on the north shore reef crest, currents can be much larger (0.1–0.3 m s^{-1}, Figures 14b and 14c). To investigate the implications of these seasonal variations for small-scale spatial flow patterns, across-reef currents were converted to effective wake lengths using the relationship in Figure 10. In the austral winter, when the wave-driven circulation is weak, wake lengths are predicted to be roughly normally distributed with a mean length of 2.5 colony diameters (Figure 14e). However, in the austral summer when the wave-driven circulation is generally stronger, the mean wake length is 4 bommie diameters. During the austral summer, wake lengths have a more skewed distribution because the incident flow is more frequently large enough that the wake length is independent of incident flow speed (Figure 14d).

[54] We observed differences in Reynolds number between seasons and therefore spatial patterns in flow should vary too. Seasonal differences in individual wake characteristics likely alter interactions between adjacent obstacles and their wakes. For example, longer wakes result in more flow sheltering and increased levels of turbulence in the flow incident on downstream obstacles. Because wake lengths vary with incident flow speed and turbulence levels, simple relationships between flow speed and net drag/turbulence (e.g., quadratic drag) may be less accurate because incident flow conditions vary as bulk flow speeds vary. This study suggests that models for drag and mixing that explicitly account for physical processes occurring on complex topography must consider the interplay of length scales such as obstacle size, obstacle spacing, wake length, and boundary layer development distance.

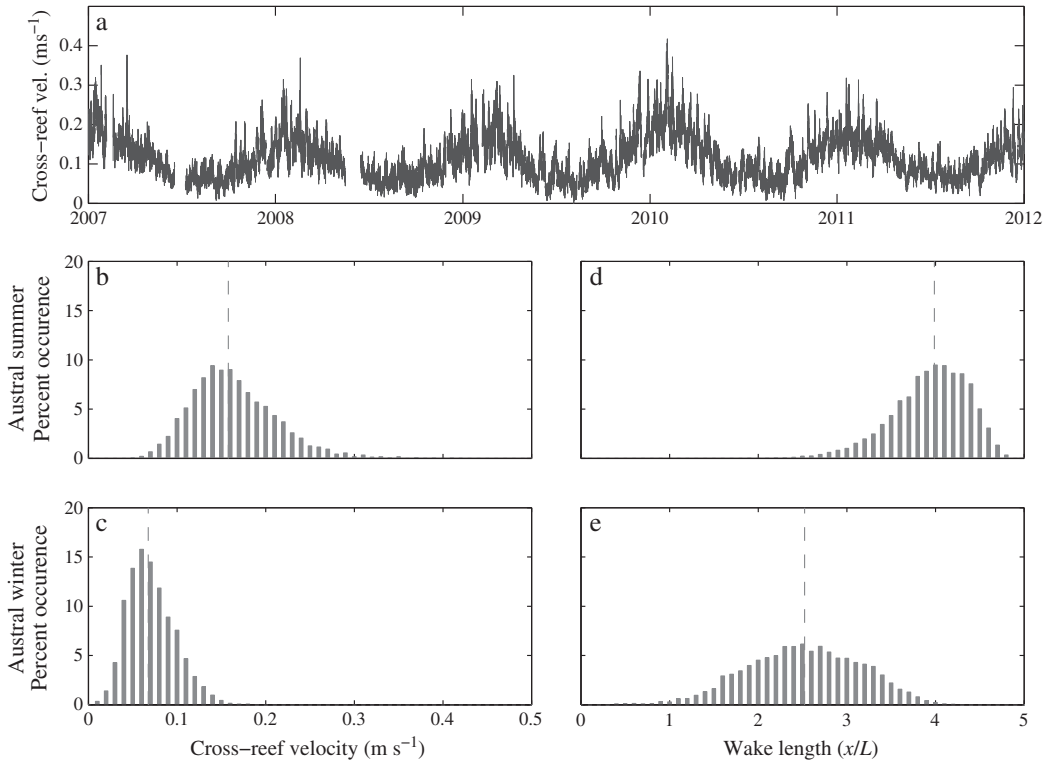

Figure 14. Seasonal differences in cross-reef velocities and corresponding wake lengths. (a) Time series of 20 min averaged cross-reef velocities collected every 2 h over a 5 year period from January 2007 through December 2011 on the backreef. (b, c) Histograms of cross-reef velocities for austral summer (December to February) and austral winter (June to August). (d, e) Wake lengths were predicted from across-reef currents using the fit in Figure 10. Vertical lines indicate medians for each season.

4.4. Implications for Reef Organisms

[55] Many questions involving physical-biological interactions are viewed as "bottom-up" processes; that is, physical processes transport dissolved and particulate materials and exert forces on organisms, thus affecting biological processes. However, organisms can profoundly affect physical processes at a range of scales by creating a rough, spatially variable substrate. Our observations indicate that on shallow reef flats there can be as much variability in currents and turbulence at scales of a few coral colonies as there is at reef scales. The complex reef structure generated by corals modifies flow patterns and turbulence; this likely has feedbacks to adjacent reef organisms.

[56] Microenvironments such as regions of strong and weak current and high and low turbulence that exist around coral colonies may be preferentially utilized by different organisms. Corals grow more rapidly in high flow environments that occur on the tops of large bommies than lower in the water column where flow speeds are slower, most likely due to greater food fluxes and higher rates of mass transfer to coral tissue [*Lenihan and Edmunds*, 2010; *Schutter et al*., 2010]. Measurements in other systems have found that algal cover and morphology can be affected by reduced flow speeds that occur behind protruding bodies and within crevices [*Ferrier and Carpenter*, 2009]. In a study of freshwater stream suspension feeders "current shading," a reduction in mean velocity in the wake of an upstream organism increased biodiversity downstream [*Cardinale et al*., 2002]. Persistent wakes behind coral colonies may have similar effects, creating niche environments downstream that shelter benthic reef organisms from drag forces. However, reduced mean flow speeds also reduce mass transfer rates, which could be detrimental to some downstream organisms. Our results suggest that organisms living in wakes of upstream organisms are subject to more vigorous velocity and scalar fluctuations and increased vertical mixing. *Falter et al*. [2007] argue that free-stream turbulence intensity over densely spaced coral colonies does not have a large effect on mass transfer rates. This many not be the case in the colony wakes considered here, which exhibited a simultaneous drop in mean flow and increase in turbulence. Additionally, spatial flow patterns are not constant with time because wake length and intensity vary as incident flow speeds vary; thus, a benthic organism could be in a different part of the wake and thus experience different conditions depending on the flow speed.

[57] The recirculation zone may retain materials close to a coral bommie, which could have positive or negative effects on the coral itself or on organisms living in its wake. Experiments on spatial patterns in feeding behavior by coral polyps have shown that particle capture shifts from upstream parts of the colony to downstream parts as flow speed increases because the feeding ability of coral polyps is inhibited in rapid flows [*Patterson*, 1984; *Helmuth and Sebens*, 1993]. In addition, the recirculation zone behind corals that forms in rapid flows may trap particles and draw them to the back of the coral, enhancing the feeding success of polyps on the downstream side of colonies. Our qualitative observations suggest that sediment eroded from in front of and beside bommies is retained in the recirculation zone and deposited within 0.5 diameters of the back of bommies in rapid flows. Thus, sedimentation that occurs during fast flows could be detrimental to organisms living within the recirculation zone of coral bommies.

[58] Spatial flow patterns at the coral colony and patch scales may also have implications for biological processes at reef scales. As dissolved and particulate materials are transported across reefs, they sample spatial variations in currents and are mixed horizontally by turbulence; therefore, the dispersion rates in both lateral (cross-flow) and longitudinal (parallel to flow) directions depend on spatial patterns in currents and turbulence [e.g., *Tanino and Nepf*, 2008]. Because spatial flow patterns vary with time, rates of dispersion may also vary with time in a way that is not easily predicted from bulk flow speeds.

5. Conclusions

[59] Our small-scale flow measurements on the Moorea backreef resolved persistent spatial patterns in currents and turbulence at scales from a single colony to several adjacent colonies. These measurements illustrate that, on shallow reef flats where coral colonies occupy a significant fraction of the water column, there can be as much spatial flow variability at colony scales as at larger scales. Currents increased by up to 50% in acceleration zones over and between colonies while flow direction reversed in recirculation eddies behind colonies. Turbulent dissipation rates in colony wakes were more than 20 times larger than upstream. While wakes behind colonies have many of the same characteristics as wakes behind simpler obstacles in idealized flows, under natural flow conditions the situation is more complicated because flow conditions vary continuously over a large range of time scales. Wake characteristics vary with time as incident flow speeds vary. Spatial flow patterns also depend on the frequency of flow variations; for example, low-frequency flow variations corresponding to Keulegan-Carpenter numbers greater than unity were reduced downstream of colonies, while higher-frequency flow variations were not significantly affected.

[60] Our scaling results suggest that forces exerted on the flow by coral colonies are significant in the spatially averaged momentum budget if obstacle spacing is similar in magnitude to obstacle diameter. In general, the dominant force acting on low-frequency flow variations is drag, while the dominant force affecting high-frequency flow variations is the inertial force. The transition from drag dominated to inertia dominated regimes depends on the Keulegan-Carpenter number and thus occurs at a higher frequency for smaller obstacles and/or larger velocity amplitudes. We were not able to explain all of the observed across-reef drag by scaling up drag forces from individual coral bommies suggesting that more complicated processes such as interactions between flow around adjacent obstacles and boundary layer adjustment to changing boundary conditions are likely important for determining net drag. Thus, there is a complex interplay between small-scale spatial variability and temporal variability that can affect both larger-scale physical and biological processes on reefs.

[61] **Acknowledgments.** We thank two anonymous reviewers for their thoughtful comments that improved the manuscript. Support for this work came from the National Science Foundation through the Moorea Coral Reef LTER (OCE-1026851) and Physical Oceanography (OCE-1061108) programs.

References

Albertson, J. D., and M. B. Parlange (1999), Surface length scales and shear stress: Implications for land-atmosphere interaction over complex terrain, *Water Resour. Res.*, *35*, 2121–2132.

Bromirski, P. D., D. R. Cayan, and R. E. Flick (2005), Wave spectral energy variability in the northeast Pacific, *J. Geophys. Res.*, *110*, C03005, doi:10.1029/2004JC002398.

Callaghan, D. P., P. Nielsen, N. Cartwright, M. R. Gourlay, and T. E. Baldock (2006), Atoll lagoon flushing forced by waves, *Coastal Eng.*, *53*, 691–704.

Cardinale, B. J., M. A. Palmer, and S. L. Collins (2002), Species diversity enhances ecosystem functioning through interspecific facilitation, *Nature*, *414*, 426–429.

Chamberlain, J. A., and R. R. Graus (1975), Water flow and hydromechanical adaptations of branched reef corals, *Bull. Mar. Sci.*, *25*, 112–125.

Chang, S., C. Elkins, M. Alley, J. Eaton, and S. Monismith (2009), Flow inside a coral colony measured using magnetic resonance velocimetry, *Limnol. Oceanogr.*, *54*, 1819–1827.

Cowen, R. K., and S. Sponaugle (2009), Larval dispersal and marine population connectivity, *Ann. Rev. Mar. Sci.*, *1*, 443–466.

Dean, R., and R. Dalrymple (1991), *Water Wave Mechanics for Engineers and Scientists*, Adv. Ser. Ocean Eng., vol. *2*, World Sci., Hackensack, N. J.

Edmunds, P. J., J. J. Leichter, and M. Adjeroud (2010), Landscape-scale variation in coral recruitment in Moorea, French Polynesia, *Mar. Ecol. Prog. Ser.*, *414*, 75–89.

Emery, W. J., and R. E. Thomson (2001), *Data Analysis Methods in Physical Oceanography*, Elsevier, Amsterdam.

Falter, J. L., M. J. Atkinson, and M. A. Merrifield (2004), Mass transfer limitation of nutrient uptake by a wave-dominated reef flat community, *Limnol. Oceanogr.*, *49*, 1820–1831.

Falter, J. L., M. J. Atkinson, R. J. Lowe, S. G. Monismith, and J. R. Koseff (2007), Effects of nonlocal turbulence on the mass transfer of dissolved species to reef corals, *Limnol. Oceanogr.*, *52*, 274–285.

Ferrier, G. A., and R. C. Carpenter (2009), Subtidal benthic heterogeneity: flow environment modification and impacts on marine algal community structure and morphology, *Biol. Bull.*, *217*, 115–129.

Gerbi, G. P., J. H. Trowbridge, J. B. Edson, A. J. Plueddemann, E. A. Terray, and J. J. Fredericks (2008), Measurements of momentum and heat transfer across the air-sea interface, *J. Phys. Oceanogr.*, *38*, 1054–1072.

Gourlay, M. R., and G. Colleter (2005), Wave-generated flow on coral reefs - an analysis for two-dimensional horizontal reef-tops with steep faces, *Coastal Eng.*, *52*, 353–387.

Hearn, C. J. (2011), Perspectives in coral reef hydrodynamics, *Coral Reefs*, *30*, 1–9.

Helmuth, B., and K. Sebens (1993), The influence of colony morphology and orientation to flow on particle capture by the scleractinian coral Agaricia agaricites (Linnaeus), *J. Exp. Mar. Biol. Ecol.*, *165*, 251–278.

Hench, J. L., J. J. Leichter, and S. G. Monismith (2008), Episodic circulation and exchange in a wave-driven coral reef and lagoon system, *Limnol. Oceanogr.*, *53*, 2681–2694.

Jaramillo, S., and G. Pawlak (2011), AUV-based bed roughness mapping over a tropical reef, *Coral Reefs*, *30*, 11–23.

Kaandorp, J. A., E. A. Koopman, P. M. A. Sloot, R. P. M. Bak, M. V. A. Vermeij, and L. E. O. Lampmann (2003), Simulation and analysis of flow patterns around the scleractinian coral Madracis mirabilis (Duchassaing and Michelotti), *Phil. Trans. R. Soc. London B*, *358*, 1551–1557.

Kundu, P. K. (1990), *Fluid Mechanics*, Academic Press, San Diego, Calif.

Lenihan, H. S., and P. J. Edmunds (2010), Response of *Pocillopora verrucosa* to corallivory varies with environmental conditions, *Mar. Ecol. Prog. Ser.*, *409*, 51–63.

Lowe, R. J., J. R. Koseff, and S. G. Monismith (2005), Oscillatory flow through submerged canopies: 1. Velocity structure, *J. Geophys. Res.*, *110*, C10016, doi:10.1029/2004JC002788.

Lowe, R. J., J. L. Falter, J. R. Koseff, S. G. Monismith, and M. J. Atkinson (2007), Spectral wave flow attenuation within submerged canopies: Implications for wave energy dissipation, *J. Geophys. Res.*, *112*, C05018, doi:10.1029/2006JC003605.

Lowe, R. J., J. L. Falter, S. G. Monismith, and M. J. Atkinson (2009a), Wave-driven circulation of a coastal reef-lagoon system, *J. Phys. Oceanogr.*, *39*, 873–893.

Lowe, R. J., J. L. Falter, S. G. Monismith, and M. J. Atkinson (2009b), A numerical study of circulation in a coastal reef-lagoon system, *J. Geophys. Res.*, *114*, C06022, doi:10.1029/2008JC005081.

Madin, J. S., and S. R. Connolly (2006), Ecological consequences of major hydrodynamic disturbances on coral reefs, *Nature*, *444*, 477–480.

Manhart, M. (1998), Vortex shedding from a hemisphere in a turbulent boundary layer, *Theoret. Comput. Fluid Dyn.*, *12*, 1–28.

Mass, T., A. Genin, U. Shavit, M. Grinsteind, and D. Tchernov (2010), Flow enhances photosynthesis in marine benthic autotrophs by increasing the efflux of oxygen from the organism to the water, *PNAS*, *107*, 2375–2724.

Meroney, R. N., C. W. Letchford, and P. P. Sarkar (2002), Comparison of numerical and wind tunnel simulation of wind loads on smooth, rough, and dual domes immersed in a boundary layer, *Wind Struct.*, *5*, 347–358.

Monismith, S. G. (2007), Hydrodynamics of coral reefs, *Annu. Rev. Fluid Mech.*, *39*, 37–55.

Nepf, H. M. (1999), Drag, turbulence, and diffusion in flow through emergent vegetation, *Water Resour. Res.*, *35*, 479–489.

Patterson, M. R. (1984), Patterns of whole colony prey capture in the octocoral Alcyonium siderium, *Biol. Bull.*, *167*, 613–629.

Patterson, M. R., K. P. Sebens, and R. R. Olsen (1991), In situ measurements of flow effects on primary production and dark respiration in reef corals, *Limnol. Oceanogr.*, *36*, 936–948.

Pope, S. B. (2000), *Turbulent Flows*, Cambridge University Press, Cambridge.

Raupach, M. R., and R. H. Shaw (1982), Averaging procedures for flow within vegetation canopies, *Boundary Layer Meteorol.*, *22*, 79–90.

Reidenbach, M. A., S. G. Monismith, J. R. Koseff, G. Yahel, and A. Genin (2006), Boundary layer turbulence and flow structure over a fringing coral reef, *Limnol. Oceanogr.*, *51*, 1956–1968.

Reidenbach, M. A., J. R. Koseff, and M. A. R. Koehl (2009), Hydrodynamic forces on larvae affect their settlement on coral reefs in turbulent, wave-driven flow, *Limnol. Oceanogr.*, *54*, 318–330.

Rosman, J. H., and J. L. Hench (2011), A framework for understanding drag parameterizations for coral reefs, *J. Geophys. Res.*, *116*, C09010, doi:10.1029/2010JC006892.

Savory, E., and N. Toy (1986), The flow regime in the turbulent near wake of a hemisphere, *Exp. Fluids*, *4*, 181–188.

Schutter, M., J. Crocker, A. Paijmans, M. Janse, R. Osinga, A. J. Verreth, and R. H. Wijffels (2010), The effect of different flow regimes on the growth and metabolic rates of the scleractinian coral Galaxea fascicularis, *Coral Reefs*, *29*, 737–748.

Sebens, K. P., S. P. Murray, and J. H. Suhayda (1998), Water flow and prey capture by three scleractinian corals, Madracis mirabilis, Montastrea cavernosa, and Porites porites in a field enclosure, *Mar. Biol.*, *131*, 347–360.

Sebens, K. P., B. Helmuth, E. Carrington, and B. Agius (2003), Effects of water flow on growth and energetics of the scleractinian coral Agaricia tenuifolia in Belize, *Coral Reefs*, *22*, 35–47.

Shaw, W. J., J. H. Trowbridge, and A. J. Williams, III (2001), Budgets of turbulent kinetic energy and scalar variance in the continental shelf bottom boundary layer, *J. Geophys. Res.*, *106*, 9551–9564.

Taniguchi, S., H. Sakamoto, M. Kiya, and M. Arie (1982), Time-averaged aerodynamic forces acting on a hemisphere immersed in a turbulent boundary layer, *J. Wind Eng. Ind. Dyn.*, *9*, 257–273.

Tanino, Y., and H. M. Nepf (2008), Lateral dispersion in random cylinder arrays at high Reynolds number, *J. Fluid Mech.*, *600*, 339–371.

Thomas, F. I. M., and M. J. Atkinson (1997), Ammonium uptake by coral reefs: Effects of water velocity and surface roughness on mass transfer, *Limnol. Oceanogr.*, *42*, 81–88.

Wyatt, A. S. J., R. J. Lowe, S. Humphries, A. M. Waite (2010), Particulate nutrient fluxes over a fringing coral reef: relevant scales of phytoplankton production and mechanisms of supply, *Mar. Ecol. Prog. Ser.*, *405*, 113–130.

Zawada, D. G., G. A. Piniak, and C. J. Hearn (2010), Topographic complexity and roughness of a tropical benthic seascape, *Geophys. Res. Let.*, *37*, L14604, doi:10.1029/2010GL043789.

Zhang, Z., J. Falter, R. Lowe, and G. Ivey (2012), The combined influence of hydrodynamic forcing and calcification on the spatial distribution of alkalinity in a coral reef system, *J. Geophys. Res.*, *117*, C04034, doi:10.1029/2011JC007603.